HHS Public Access

Author manuscript

Analyst. Author manuscript; available in PMC 2017 April 11.

Published in final edited form as:

Analyst. 2016 April 21; 141(8): 2418–2425. doi:10.1039/c6an00123h.

Quantitative imaging of 2 nm monolayer-protected gold nanoparticle distributions in tissues using laser ablation inductively-coupled plasma mass spectrometry (LA-ICP-MS)

S. Gokhan Elci[a], **Bo Yan**[a], **Sung Tae Kim**[a], **Krishnendu Saha**[a], **Ying Jiang**[a], **Gunnar A. Klemmer**[b], **Daniel F. Moyano**[a], **Gulen Yesilbag Tonga**[a], **Vincent M. Rotello**[a], and **Richard W. Vachet**[a,*]

[a]Deparment of Chemistry, University of Massachusetts, 710 North Pleasant Street, Amherst, MA, 01002

[b]Department of Chemistry, Harding University, 915 East Market Avenue, Searcy, AR, 72149

Abstract

Functionalized gold nanoparticles (AuNPs) have unique properties that make them important biomedical materials. Optimal use of these materials, though, requires an understanding of their fate *in vivo*. Here we describe the use of laser ablation inductively coupled plasma mass spectrometry (LA-ICP-MS) to image the biodistributions of AuNPs in tissues from mice intravenously injected with AuNPs. We demonstrate for the first time that the distributions of very small (~ 2 nm core) monolayer-protected AuNPs can be imaged in animal tissues at concentrations in the low parts-per-billion range. Moreover, the LA-ICP-MS images reveal that the monolayer coatings on the injected AuNPs influence their distributions, suggesting that the AuNPs remain intact *in vivo* and their surface chemistry influences how they interact with different organs. We also demonstrate that quantitative images of the AuNPs can be generated when the appropriate tissue homogenates are chosen for matrix matching. Overall, these results demonstrate the utility of LA-ICP-MS for tracking the fate of biomedically-relevant AuNPs *in vivo*, facilitating the design of improved AuNP-based therapeutics.

TOC image

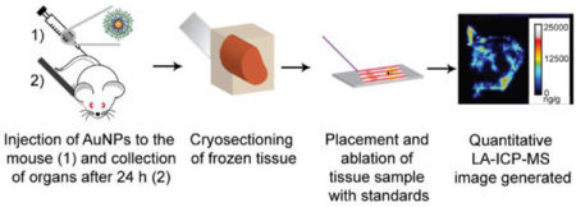

[*]**Corresponding Author:** Richard W. Vachet, Department of Chemistry, 240 Thatcher Way, Life Sciences Laboratory, N363, University of Massachusetts Amherst, Amherst, MA 01003, rwvachet@chem.umass.edu.

Note

The authors declare no competing financial interest

Introduction

Nanomaterials are widely used in biomedical applications such as drug delivery, therapeutics, sensors and other nanodevices.[1,2,3] Functionalized nanoparticles (NPs) have tailorable sizes and surface properties that allow them to be tuned for a wide range of biomedical applications. For example, NP surface chemistry can be designed to influence their absorption, distribution, metabolism, excretion, and toxicity.[4,5] Gold NPs (AuNPs), in particular, have been widely studied because they possess unique qualities that make them appealing for biomedical applications. Gold is inherently non-toxic. AuNPs can be readily synthesized to have a range of sizes, and their surface properties can be easily modified by taking advantage of gold-thiol chemistry.[6,7] In recent years, there has been a rapid increase in the use of AuNPs in drug delivery,[8] sensing,[3] cancer diagnosis and therapy,[9] and even environmental studies.[10,11]

Several approaches have been applied to understand the fate of the AuNPs *in vivo*. A commonly used approach is surface-enhanced Raman spectroscopy (SERS), which relies on the plasmonic properties of AuNPs and how these properties change during interactions with each other and with biological systems.[12,13,14,15] The use of SERS for quantitation, however, has been very limited. Electron microscopy is commonly used to image NPs in biological samples. This technique is typically low throughput, though, and does not broadly lend itself to reliable quantitative information, despite some recent nanopipette-based approaches to address this issue.[16] X-ray spectroscopies have also been used to image AuNPs[17,18] and other NPs,[19,20] but these techniques require difficult to access instrumentation such as synchrotron sources.

Laser ablation inductively coupled plasma mass spectrometry (LA-ICP-MS) is an emerging method for imaging NP distributions in biological systems[21,22,23] This technique has high sensitivity, multi-element detection capability, and spatial resolutions in the 25–50 μm range that make it suitable for tissue analyses. In addition, quantitative images can be obtained when using the appropriate standardization approaches.[24,25,26] To date, several reports have described the imaging of nanomaterials in cells,[27,28,29] tissues[30,31,32] and plants.[33] A few of these studies have involved AuNPs, yet all but one[33] have measured AuNPs with core sizes between 13 and 50 nm. AuNPs with smaller core sizes (< 5 nm) are biomedically interesting because these systems have high payload to carrier ratios. Also, together with their monolayer coatings these NPs are just large enough to avoid being cleared by the kidney but small enough to have sufficient circulation times for therapeutic applications.[34] The challenge of detecting and imaging these smaller AuNPs, however, is the fact that they contain much less gold than their larger counterparts. For example, a AuNP with a 2 nm core diameter has 1000 times less gold than a AuNP with a 20 nm core.

In this work, we demonstrate the quantitative imaging of functionalized AuNPs with 2 nm cores. To our knowledge, this work represents the first example of quantitative imaging of such small AuNPs in animal tissues. We show that LA-ICP-MS imaging provides sub-tissue biodistribution information that is valuable for understanding the biological fate of AuNPs *in vivo*. Moreover, we find that the AuNPs remain intact *in vivo* as different surface monolayers cause distinct sub-tissue distributions. Overall, these measurements open the

door for studying how surface chemistry influences AuNP biodistributions, with important implications for the design of NP-based therapeutics.

Experimental Section

Synthesis of 2 nm AuNPs

The AuNPs used in this study (Figure 1) were synthesized by the Brust-Schiffrin two-phase method, and were post-functionalized using the Murray place exchange reaction.[35,36] The details of the synthetic procedure for the NPs used in this study are reported in previous work.[37,38,39] After synthesis, the AuNPs were dialyzed for 72 h against MilliQ water using Spectra/Por Dialysis Membranes (molecular weight cutoff of 1,000 Da) to separate the free ligands from the AuNPs. The core sizes of the NPs were then measured by transmission electron microscopy (TEM) on a JEOL100S electron microscope and were found to have core diameters that are 2.0 ± 0.1 nm, 1.8 ± 0.2 nm and 2.0 ± 0.4 nm for AuNP 1, 2, and 3, respectively (Figure S1 in the Supporting Information). They were also characterized by laser-desorption/ionization mass spectrometry to confirm the monolayer coating.[40]

Animal Experiments

Animal care—All animal experiments were conducted in accordance with the guidelines of Institutional Animal Care and Use Committee (IACUC) at University of Massachusetts Amherst. Female Balb/c mice were purchased from Jackson Laboratory (Bar Harbor, ME). Food and water intake were assessed daily.

Intravenous injection of AuNPs—50 μL of each AuNP at a concentration of 2 μM was administered intravenously to the Balb/c mice. Because the average NP core sizes are about 2 nm, the total gold amount of injected in case was approximately 4000 ng, which is expected given that around 200 gold atoms are present in each AuNP.[41] After 24 h, the mice were sacrificed by the inhalation of carbon dioxide and cervical dislocation. The organ samples were then harvested for analysis. Following sacrifice, organs were collected and cut into two parts, except the kidneys and lungs of which each mouse has two. One part or one of the duplicate organs (in the case of the lung and kidney) was homogenized and analyzed by ICP-MS for total gold, while the other was used for LA-ICP-MS imaging.

Tissue preparation for imaging—Using a LEICA CM1850 cryostat, tissue samples were sliced to a thickness of 12 μm (for spleen and liver) or 20 μm (for kidney and lung) at −20 °C. Then, the sliced tissues were attached to regular glass slides.

ICP-MS sample preparation and measurements

Using a 3:1 (v:v) mixture of HNO_3 (68%) and H_2O_2 (30%), each organ was digested overnight. The next day 0.5 mL of aqua regia was added, and the sample was then diluted to 10 mL using de-ionized water. (**Aqua regia is highly corrosive and must be handled with extreme caution.**) Au standard solutions (gold concentrations: 20, 10, 5, 2, 1, 0.5, 0.2 and 0 ppb) were prepared prior to each experiment. A Perkin Elmer NEXION 300X ICP mass spectrometer was used for the analysis of samples. Prior to the analysis, daily performance measurements were done to ensure the instrument was operating under optimum conditions.

Using the standard mode, ^{197}Au signals were obtained. The RF power for the ICP was 1.6 kW, and the nebulizer gas flow rate was within a range of 0.9–1 L/min. The plasma gas flow rate and auxiliary gas flow rate were 16.5 L/min and 1.4 L/min, respectively. The analog stage voltage and pulse stage for the detector were −1600 V and 950 V, respectively. The deflector voltage was set to −12 V, and 50 ms was selected for the dwell time during the operation of the ICP-MS.

LA-ICP-MS measurement conditions and imaging

For imaging of the tissue samples, a CETAC LSX-213 G2 laser ablation system (Photon Machines, Omaha, NE, USA) attached via a 2 m length of tubing to the ICP mass spectrometer was used. Optimization of the laser ablation conditions was first performed using pure AuNP samples on glass slides. As described in the results and discussion, the optimal conditions were found to be: a laser energy of 3.34 J, a spot size of 50 μm, a scan rate of 10 μm/sec, and laser shot frequency of 10 Hz. The laser energy value was obtained directly from the indicator on the CETAC laser ablation system. Laser scanning was done in the line scan mode. Transfer of the ablated material from the ablation chamber to the plasma was accomplished using a 600 mL/min flow of He gas and a 10 sec shutter delay. The mass spectrometer was operated using the kinetic energy discrimination mode, which was especially important for measurements of ^{57}Fe.

Data analysis and image generation

ICP-MS data were analyzed using Excel and Origin 9.0 (from OriginLab, Northampton, MA, USA). Excel was used to process the data acquired during the line scan mode in a manner similar to that used previously.[42] In short, individual pixel images with a size of 50 μm × 50 μm were obtained by summing 5-second increments of data collected at a scan rate of 10 μm/s. Upon processing the data via Excel, images were rendered using the software ImageJ. Optical images of the tissues were processed with Adobe Photoshop.

Matrix-matched standard preparation for LA-ICP-MS

Chicken breast and beef liver were purchased from a local market and used as the matrix-matched standards. Small pieces of these tissues were cut and placed in 15 mL plastic tubes. Water was added to the tubes, and the tissues were homogenized using a PowerGen 125 homogenizer (Fisher Scientific). Homogenized tissues were transferred into 1.5 mL centrifuge tubes and were centrifuged at 12000 rpm for 10 minutes. Using a pipette, excess water in the supernatant was removed from each centrifuge tubes, and 50 mg homogenates were weighed and transferred into 0.5 mL tubes. 50 μL of 2 μM AuNP solutions were then mixed with the 50 mg homogenates. The AuNP-homogenates mixtures were then placed into a homemade sample holder and frozen prior to slicing at the desired thickness on the cryostat. Details of sample holder preparation can be found in the Supporting Information.

Results and Discussion

Three different AuNPs (Figure 1, AuNPs 1–3) were selected to investigate the ability of LA-ICP-MS to image AuNPs in mouse tissues. The AuNPs consist of a 2 nm Au core (Figure S1) and monolayers attached to the core via a thiol group (Figure 1). The design of the

monolayer structure provides biocompatibility, solubility in water and stability for these AuNPs.[8] Indeed, previous studies have shown that this NP design is biocompatible in fish and mice[43,44,45] and that this design allows the NPs to remain intact *in vivo*.[45] Spleen, liver, lung, and kidney tissues were selected for imaging because separate ICP-MS experiments on tissue homogenates indicated that these tissues were the main sites of Au accumulation after NP injection (Table 1). Moreover, these organs represent a range of tissue types with various sub-tissue features.

To arrive at the optimal parameters for quantitative laser ablation analysis of the AuNPs, we deposited AuNPs on glass slides using an inkjet printer in a manner similar to that described previously.[46] Laser energy, frequency, scan rate, and spot size were investigated, and laser energy and scan rate were found to be particularly important for obtaining homogeneous Au signals for images with optimal resolution (Figure S2). Laser conditions that gave relatively constant ion signals over a 500 μm space of inkjet-printed AuNPs tended to provide the best tissue images. We found that the best images were obtained with a laser energy of 3.34 J (40% power) and a scan rate of 10 μm/sec, which is slower than most LA-ICP-MS imaging applications that typically use a scan rate above 30 μm/sec.

Upon identifying optimal imaging conditions, we first examined spleen tissues because their distinct histological regions (i.e. red pulp and white pulp) are particularly revealing about the value of LA-ICP-MS imaging (Figure 2). The spleen also plays a major role in filtering the blood, which likely explains the high concentration of NPs found in this organ. From Figure 2, it is clear that Au accumulates in the red pulp region (i.e. red/orange color in optical image of Figure 2a and less dense purple color in the H&E stains shown in Figure S3) but not in the white pulp region (i.e. white circles in optical image of Figure 2a, pale red regions in the ^{57}Fe images in Figure 2c, and more dense purple color in the H&E stains shown in Figure S3) of the tissue after injection of AuNP 1. The role of the red pulp is to remove antigens, microorganisms and dead erythrocytes from the blood, while the white pulp contains different lymphocytes that are important in immune responses. These images suggest that AuNP 1 is filtered from circulation but is not taken up by the lymphocytes that comprise the white pulp.

LA-ICP-MS images of spleens taken from mice injected with AuNPs 2 and 3 are also readily obtained (Figure 3), even though these AuNPs accumulate in the spleen to a much lesser extent than AuNP 1 (Table 1). The images in Figure 3 illustrate that the red pulp is the primary site of accumulation for both NPs; however, AuNP 2 clearly distributes to some extent in the white pulp as well. This observation is in stark contrast to the behavior of AuNPs 1 and 3, indicating that NP surface chemistry influences how the NPs distribute internally. Importantly, because the different AuNPs show different distributions, the NPs very likely remain intact *in vivo*, highlighting the fact that our measurements are reporting on the AuNP distributions and not just total gold. Independent validation of this conclusion is difficult given the dearth of tools capable of measuring intact NPs in complex tissues, but previous work indicates that the AuNPs used here are likely to remain intact in vivo. AuNPs with the same design were shown to be stable inside cells for up to 24 h,[47] and AuNP 1 was shown to be intact for up to 24 h after injection into mice.[45]

We were also able to obtain valuable images from liver, kidney, and lung tissues (Figure 4). The liver, which typically accumulates the second highest level of AuNPs in our experiments (Table 1), is responsible for removing toxic substances from circulation by storing or detoxifying them. In general, the liver shows a more homogeneous distribution of AuNPs than the spleen; however, we do find that AuNP 1 accumulates more in liver tissue surrounding the blood vessels rather than in the blood vessels themselves (Figure 4b). This observation can be confirmed by comparing the images of the Au distributions with the images of ^{57}Fe distributions (Figure 4c). Fe is more homogeneously distributed throughout the liver tissue, including in the blood vessels. Significant levels of Au are not found in the blood vessels, suggesting rapid uptake of AuNP 1 into the surrounding tissue and clearance from circulation. Interestingly, AuNPs 2 and 3 show a broader distribution throughout the liver, including in the blood vessels (Figure S4). The fact that AuNPs with different surface chemistries distribute differently highlights that these images are revealing AuNP distributions and not just bulk gold distributions.

Somewhat surprisingly we also find AuNPs in lung tissue, even though the NPs were injected intravenously (Figure 4d and e). The presence of gold in this tissue is likely due to the large amount of blood circulating through the lungs to remove gaseous molecules. Presumably, the AuNPs are taken up by the tissue surrounding the alveolar spaces, which are seen as black in the optical image of Figure 4d. Lastly, we have also obtained images of kidney tissues (Figure 4f and g), which is remarkable in that these tissues typically accumulated less than 100 ppb of Au as determined from the tissue homogenate samples (Table 1). While the Au levels are low in the kidney, it is clear that Au is found concentrated in certain regions of the kidney. The relatively low concentrations in the kidney likely reflect the fact that this organ typically filters particles that are smaller than 5 nm in size.[48] While the AuNPs used here have 2-nm cores, the monolayer of ligands makes the full AuNP sizes closer to 10 nm,[45] making their removal by the kidney less likely. Given this fact, the full implications of some locally high concentrations in the kidney are not clear.

Having established that LA-ICP-MS can indicate the distributions of functionalized 2 nm AuNPs in mouse tissues, we next investigated the possibility of generating quantitative images. To achieve this quantitation, we investigated a matrix-matching approach in which we spiked known concentrations of AuNPs into sets of tissue homogenates (Scheme S1). Ideally, appropriate mouse tissues would be used as the matrix for the organs of interest, but the small size of mouse organs and the unnecessary sacrifice of mice caused us to study more readily available tissues. We investigated chicken breast and beef liver as tissue phantoms for matrix matching and found that chicken breast worked well as a matrix match for the spleen, kidney and lung, whereas beef liver was more appropriate for liver tissues.

Using the matrix-matching strategy we were able to quantify AuNP distributions in tissues. Figure 5 shows the data for spleen tissue from a mouse that was injected with AuNP 3. Using chicken breast homogenate, we obtained the calibration curve for the spleen tissue using five different NP concentrations (Figure 5a). The calibration curve was obtained by averaging the Au signal from the entire tissue homogenate slice, and then this curve was used to obtain quantitative images for the spleen (Figure 5b). As was seen in Figure 3b, AuNP 3 is distributed solely in the red pulp, but now AuNP amounts at specific locations are

apparent. Site-specific quantitation is particularly valuable for spleen images of AuNP 2 (Figure 5c), which show significant levels of Au in the white pulp regions. The quantitative images indicate that 50 ± 25 ppb (or about 10%) of the NPs is found in the white pulp regions, whereas 300 ± 80 ppb (or about 60%) is found in the red pulp and a remarkable 150 ± 50 (or about 30%) is found in the one pixel-wide regions that surrounds each white pulp region. This latter narrow (~ 40 μm) region around the white pulp is known as the marginal zone and is the location where the spleen's immune response is initiated.[49] The full implications of these results are beyond the scope of this work and will be investigated in future work.

To help validate these data, we compared the average quantity obtained across this entire spleen slice to a part of the same spleen tissue that had been homogenized and analyzed by ICP-MS. In doing so, we find that the average Au amount in the tissue slice is within a factor of 2 of the tissue homogenates (Table 2). This level of agreement is excellent, given that the tissue slice represents only a very small fraction of this heterogeneous tissue, whereas the ICP-MS results were obtained from approximately one half of the entire spleen tissue.

Quantitative images were also obtained for several other tissues and NPs. For the spleen, lung, and kidney we find good agreement between the LA-ICP-MS data and the ICP-MS results from the tissue homogenates when chicken breast is used as the calibration matrix (Table 2). For liver tissues, chicken breast was not found to be a reliable matrix for quantification, as the LA-ICP-MS and ICP-MS results usually did not compare well (Tables 1 and 2). Instead, beef liver homogenates were found to be a more reliable matrix, allowing for a more reasonable comparison between the LA-ICP-MS and ICP-MS results (Tables 1 and 2). Upon applying the appropriate calibration curves for each tissue, we are able to estimate detection limits for this LA-ICP-MS imaging method. Gold amounts around 10 ng/g (i.e. 10 ppb) or higher in tissue sections provide useful quantitative information, as is evident in the images of kidney tissue (Figure 6 and Table 1). This concentration is similar to the detection range seen in previous LA-ICP-MS of transition metals, which were found to be detectable in the 10 – 300 ng/g (i.e. 10 – 300 ppb) range.[21]

Conclusion

In this work, we demonstrate that LA-ICP-MS can be used to quantitatively image the biodistributions of monolayer-protected AuNPs with 2 nm cores. To our knowledge, this is the first report on quantification of < 10 nm core AuNPs in animal tissues using LA-ICP-MS. We achieve excellent sensitivity and spatial resolution in these imaging experiments, allowing us to determine how AuNPs with different monolayer coatings distribute *in vivo*. Thus, our approach provides useful insight into not only how NPs distribute but also how they are processed *in vivo*. This latter information is accessible from the sub-organ NP distributions in tissues such as the spleen and liver. We also find that the proper choice of matrix for the calibration standards is essential for obtaining quantitative images. Taken together, this imaging approach will provide important tissue/organ distribution data that will greatly facilitate the design and study of nanomaterials for biomedical applications.

Supplementary Material

Refer to Web version on PubMed Central for supplementary material.

Acknowledgments

This work was supported by the NSF through the Center for Hierarchical Manufacturing (NSF CMMI-1025020) and via NSF CHE-1506725. V.M.R also acknowledges support from the NIH (EB014277). The authors thank Prof. Joseph Jerry for assistance with the animal studies.

References

1. Sun T, Zhang YS, Pang B, Hyun DC, Yang M, Xia Y. Angew Chem Int Ed. 2014; 53:12320–12364.
2. Lee D-E, Koo H, Sun I-C, Ryu JH, Kim K, Kwon IC. Chem Soc Rev. 2012; 41:2656–2672. [PubMed: 22189429]
3. Saha K, Agasti SS, Kim C, Li X, Rotello VM. Chem Rev. 2012; 112(5):2739–2779. [PubMed: 22295941]
4. Zolnik BS, Sadrieh N. Adv Drug Deliver Rev. 2009; 61:422–427.
5. Kim ST, Saha K, Kim C, Rotello VM. Acc Chem Res. 2013; 46:681–691. [PubMed: 23294365]
6. Boisselier E, Astruc D. Chem Soc Rev. 2009; 38:1759–1782. [PubMed: 19587967]
7. Yeh YC, Creran B, Rotello VM. Nanoscale. 2012; 4:1871–1880. [PubMed: 22076024]
8. Rana S, Bajaj A, Mout R, Rotello VM. Adv Drug Deliver Rev. 2012; 64:200–216.
9. Yesilbag Tonga G, Moyano DF, Kim CS, Rotello VM. Curr Opin Colloid Interface Sci. 2014; 19:49–55. [PubMed: 24955019]
10. Farre M, Sanchis J, Barcelo D. Trend Anal Chem. 2011; 30(3):517–527.
11. Zhu Z-J, Wang H, Yan B, Zheng H, Jiang Y, Miranda OR, Rotello VM, Xing B, Vachet RW. Environ Sci Technol. 2012; 46:12391–12398. [PubMed: 23102049]
12. Drescher D, Kneipp J. Chem Soc Rev. 2012; 41:5780–5799. [PubMed: 22782372]
13. Ando J, Fujita K, Smith NI, Kawata S. Nano Lett. 2011; 11:5344–5348. [PubMed: 22059676]
14. Qian XM, Nie SM. Chem Soc Rev. 2008; 37:912–920. [PubMed: 18443676]
15. Jain PK, Huang X, El-Sayed IH, El-Sayed MA. Accounts Chem Res. 2008; 41:1578–1586.
16. Tai L-A, Kang Y-T, Chen Y-C, Wang Y-C, Wang Y-J, Wu Y-T, Liu K-L, Wang C-Y, Ko Y-F, Chen C-Y, Huang N-C, Chen J-K, Hsieh Y-F, Yew T-R, Yang C-S. Anal Chem. 2012; 84:6312–6316. [PubMed: 22816618]
17. Xiang Li X, Anton N, Zuber G, Vandamme T. Adv Drug Deliver Rev. 2014; 76:116–133.
18. Ricketts K, Guazzoni C, Castoldi A, Gibson AP, Royle GJ. Phys Med Biol. 2013; 58:7841–7855. [PubMed: 24145214]
19. Hernandez-Viezcasa JA, Castillo-Michel H, Servin AD, Peralta-Videa JR, Gardea-Torresdey JL. Chem Eng J. 2011; 170:346–352. [PubMed: 22820414]
20. Priester JH, Ge Y, Mielke RE, Horst AM, Cole Moritz S, Espinosa K, Gelb J, Walker SL, Nisbet RM, An Y-J, Schimel JP, Palmer RG, Hernandez-Viezcas JA, Zhao L, Gardea-Torresdey JL, Holden PA. Proc Natl Acad Sci. 2012; 109:2451–2456.
21. Becker JS, Becker JS. Biomedical Spectroscopy and Imaging. 2012; 1:187–204.
22. Becker JS. Int J Mass Spectrom. 2010; 289:65–75.
23. Becker JS, Matusch A, Wu B. Anal Chim Acta. 2014; 835:1–18. [PubMed: 24952624]
24. Hare D, Austin C, Doble P. Analyst. 2012; 137:1527–1537. [PubMed: 22314636]
25. Konz I, Fernández B, Fernández ML, Pereiro R, Sanz-Medel A. Anal Bioanal Chem. 2012; 403:2113–2125. [PubMed: 22543715]
26. Hare DJ, Lear J, Bishop D, Beavis A, Doble PA. Anal Methods. 2013; 5:1915–1921.
27. Wang M, Zheng LN, Wang B, Chen HQ, Zhao YL, Chai ZF, Reid HJ, Sharp BL, Feng WY. Anal Chem. 2014; 86:10252–10256. [PubMed: 25225851]

28. Drescher D, Giesen C, Traub H, Panne U, Kneipp J, Jakubowski N. Anal Chem. 2012; 84:9684–9688. [PubMed: 23121624]
29. Büchner T, Drescher D, Traub H, Schrade P, Bachmann S, Jakubowski N, Kneipp J. Anal Bioanal Chem. 2014; 406:7003–7014. [PubMed: 25120183]
30. Wang T, Hsieh H, Hsieh Y, Chiang C, Sun Y, Wang C. Anal Bioanal Chem. 2012; 404:3025–3036. [PubMed: 23052863]
31. Hsieh YK, Hsieh HA, Hsieh HF, Wang TH, Ho CC, Lin PP, Wang CF. J Anal At Spectrom. 2013; 28:1396–1401.
32. Kamaly N, Pugh JA, Kalber TL, Bunch J, Miller AD, McLeod CW, Bell JD. Mol Imaging Biol. 2010; 12:361–366. [PubMed: 19921340]
33. Koelmel J, Leland T, Wang H, Amarasiriwardena D, Xing B. Environ Pollut. 2013; 174:222–228. [PubMed: 23277326]
34. Petros R, DeSimone J. Nat Rev Drug Discovery. 2010; 9:615–627. [PubMed: 20616808]
35. Brust M, Walker M, Bethell D, Schiffrin DJ, Whyman RJ. Chem Soc Chem Comm. 1994:801–802.
36. Templeton AC, Wuelfing MP, Murray RW. Acc Chem Res. 2000; 33:27–36. [PubMed: 10639073]
37. Miranda OR, Li XN, Garcia-Gonzalez L, Zhu ZJ, Yan B, Bunz UHF, Rotello VM. J Am Chem Soc. 2011; 133:9650–9653. [PubMed: 21627131]
38. Miranda OR, Chen HT, You CC, Mortenson DE, Yang XC, Bunz UHF, Rotello VM. J Am Chem Soc. 2010; 132:5285–5289. [PubMed: 20329726]
39. Hong R, Emrick T, Rotello VM. J Am Chem Soc. 2004; 126:13572–13573. [PubMed: 15493887]
40. Yan B, Zhu ZJ, Miranda OR, Chompoosor A, Rotello VM, Vachet RW. Anal Bioanal Chem. 2010; 396:1025–1035. [PubMed: 19911174]
41. Liu X, Atwater M, Wang J, Huo Q. Colloids and Surfaces B: Biointerfaces. 2007; 58:3–7. [PubMed: 16997536]
42. Köppen C, Reifschneider O, Castanheira I, Sperling M, Karst U, Ciarimboli G. Metallomics. 2015; 7:1595–1603. [PubMed: 26477751]
43. Zhu ZJ, Carboni R, Quercio MJ, Yan B, Miranda OR, Anderton DL, Arcaro KF, Rotello VM, Vachet RW. Small. 2010; 6:2261–2265. [PubMed: 20842664]
44. Arvizo RR, Miranda OR, Moyano DF, Walden CA, Giri K, Bhattacharya R, Robertson JD, Rotello VM, Reid JM, Mukherjee P. PLoS One. 2011; 6:e24374. [PubMed: 21931696]
45. Yan B, Kim ST, Kim CS, Saha K, Moyano DF, Xing Y, Jiang Y, Roberts AL, Alfonso FS, Rotello VM, Vachet RW. J Am Chem Soc. 2013; 135:12564–12567. [PubMed: 23931011]
46. Creran B, Yan B, Moyano DF, Gilbert MM, Vachet RW, Rotello VM. Chem Comm. 2012; 48:4543–4545. [PubMed: 22466433]
47. Zhu Z-J, Tang R, Yeh Y-C, Miranda OR, Rotello VM, Vachet RW. Anal Chem. 2012; 8:4321–4326. [PubMed: 22519403]
48. Choi HS, Liu W, Misra P, Tanaka E, Zimmer JP, Ipe BI, Bawendi MG, Frangioni JV. Nature Biotechnology. 2007; 25:1165–1170.
49. Mebius RE, Kraal G. Nature Reviews Immunology. 2005; 5:606–616.

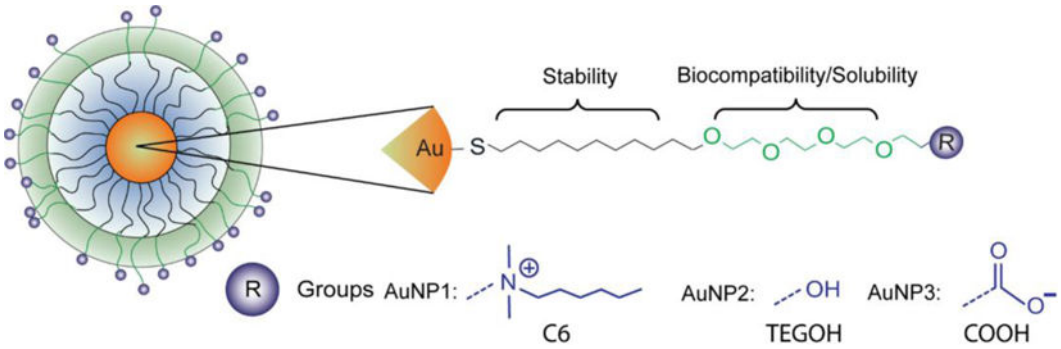

Figure 1.
Structures of AuNPs used in this study.

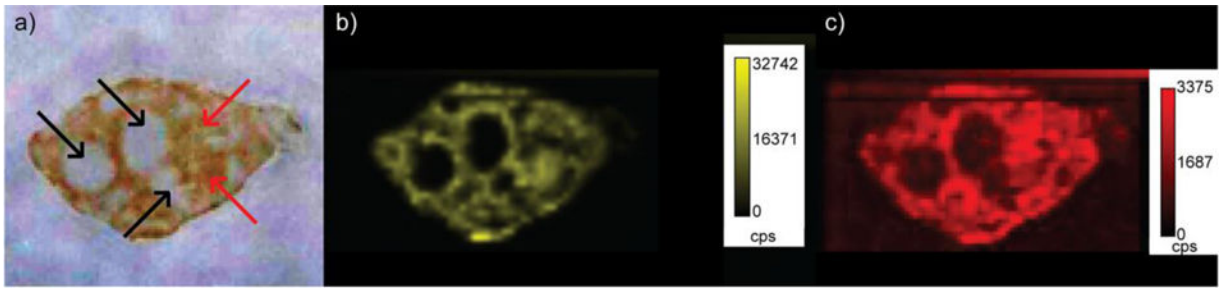

Figure 2.

a) Optical image of a spleen tissue taken from a mouse injected with AuNP 1. The red pulp is red/orange in color, whereas the white pulp is white and can be challenging to distinguish from the area surrounding the organ in this image. Selected red pulp regions are indicated with red arrows, whereas selected white pulp regions are indicated with black arrows. b) LA-ICP-MS image of the same spleen showing the distribution of gold. c) LA-ICP-MS image of the same spleen showing the distribution of the iron. (cps = counts per second)

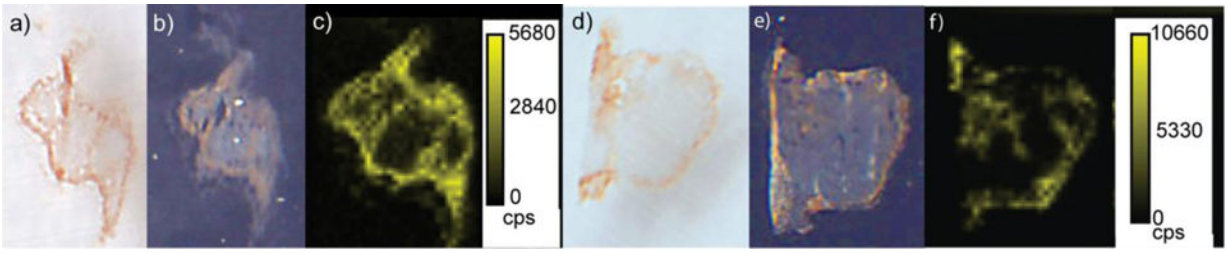

Figure 3.

a) Optical image of a spleen tissue taken from a mouse injected with AuNP 2. b) False color optical image of a spleen tissue taken from a mouse injected with AuNP 2. c) LA-ICP-MS image of the same spleen tissue showing the distribution of gold. The light gray regions indicate the white pulp. d) Optical image of a spleen tissue taken from a mouse injected with AuNP 3. e) False color optical image of a spleen tissue taken from a mouse injected with AuNP 3. The light gray regions indicate the white pulp. f) LA-ICP-MS image of the same spleen tissue showing the distribution of gold. (cps = counts per second)

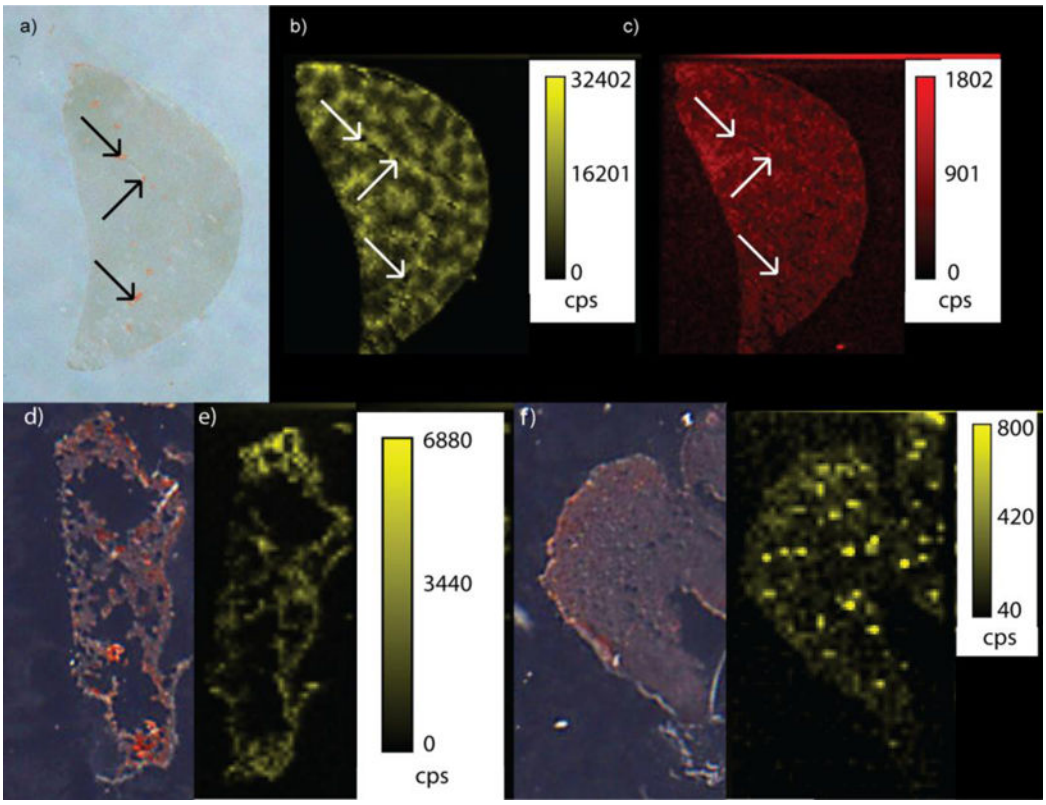

Figure 4.

a) Optical image of a liver tissue taken from a mouse injected with AuNP 1. The red spots in the optical image represent the blood vessels that traverse through the liver (black arrows indicate the portal veins present. b) LA-ICP-MS image of the same liver showing the distribution of gold. c) LA-ICP-MS image of the liver showing the distribution of Fe. d) Optical image of a lung tissue taken from a mouse injected with AuNP 1. e) LA-ICP-MS image of the same lung tissue showing the distribution of gold. f) Optical image of a kidney tissue taken from a mouse injected with AuNP 1. g) LA-ICP-MS image of the same kidney tissue showing the distribution of gold. (cps = counts per second)

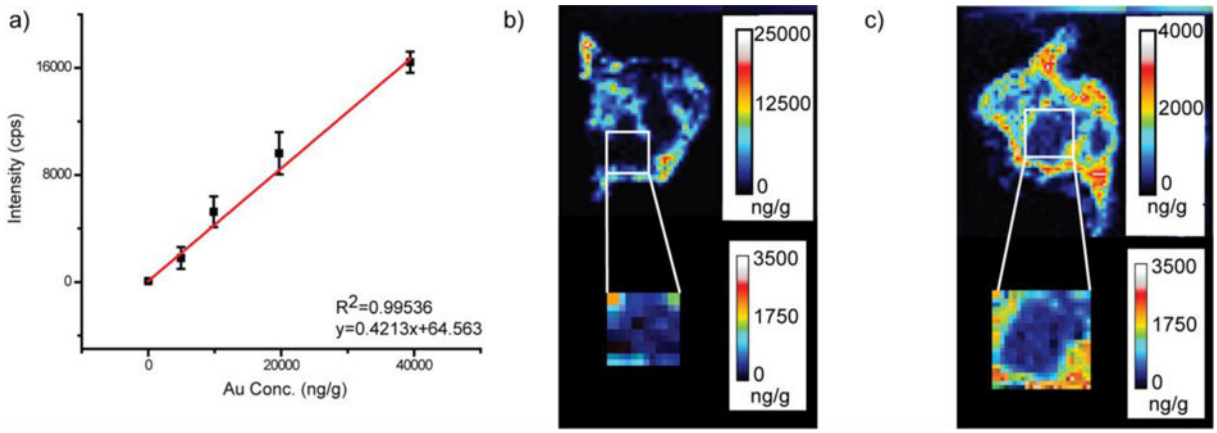

Figure 5.

a) Example calibration curve obtained for AuNP 3 using chicken breast homogenate as the matrix. b) Quantitative LA-ICP-MS image of a spleen taken from a mouse injected with AuNP 3. c) Quantitative LA-ICP-MS image of a spleen taken from a mouse injected with AuNP 2.

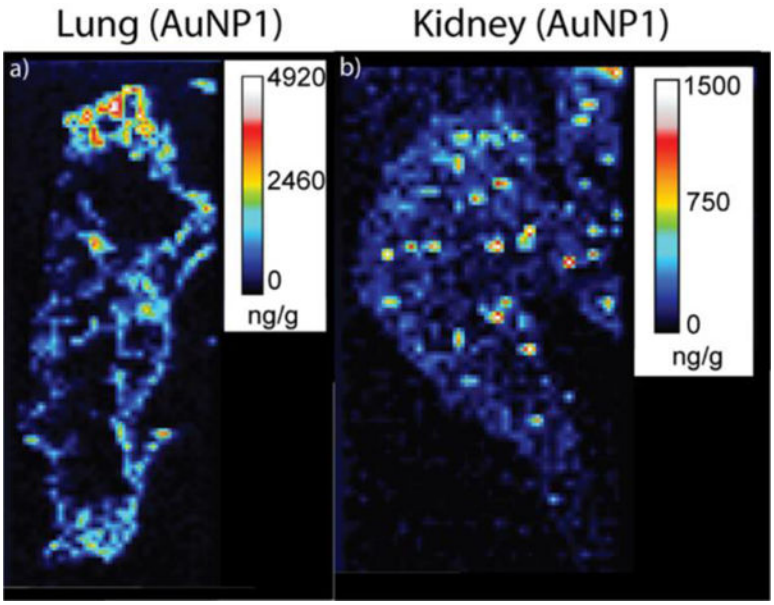

Figure 6.
Quantitative LA-ICP-MS images of a lung (a) and a kidney (b) taken from a mouse injected with AuNP1.

Table 1

Summary of ICP-MS quantification of homogenized tissue samples from mice injected with AuNPs.

	ICP-MS (ng/g)[a]			
Mouse Tissue	**AuNP 1**	**AuNP 2**	**AuNP 3[b]**	**Control**
Spleen	6000 ± 400	600 ± 100	1200 ± 300	8 ± 1
Liver	3400 ± 400	1000 ± 200	2600 ± 500	2 ± 1
Lung	700 ± 100	110 ± 40	40 ± 5	3 ± 2
Kidney	60 ± 30	55 ± 10	60 ± 5	2 ± 1

[a] The standard deviations (n = 3) are obtained by averaging the ICP-MS results obtained from three different mice injected with the indicated NP.

[b] The standard deviations (n = 2) are obtained by averaging the ICP-MS results obtained from two different mice injected with the indicated NP (Three mice were initially injected with AuNP 3, but the injection into one of these mice was not successful, and so the data from this mouse is not included).

Table 2

Summary of LA-ICP-MS quantification results of tissues slices from mice injected with AuNPs.

Mouse Tissue	LA-ICP-MS (ng/g)[a]
Spleen (AuNP1)	9000±2000 *
Spleen (AuNP2)	500±150 **
Spleen (AuNP3)	6000±4000 **
Liver (AuNP1-liver homogenate)	10000
Liver (AuNP2-chicken breast homogenate)	11000
Liver (AuNP2-liver homogenate)	450
Liver (AuNP3-liver homogenate)	3700
Lung (AuNP1)	300
Kidney (AuNP1)	80

[a]The LA-ICP-MS quantitative data obtained by summing the data obtained for each pixel.

*n=2

**n=3